N93-19414
51-13
128434
P-20

Precise Tracking of the Magellan and Pioneer Venus Orbiters by Same-Beam Interferometry Part I: Data Accuracy Analysis

J. S. Border, W. M. Folkner, R. D. Kahn, and K. S. Zukor
Tracking Systems and Applications Section

Simultaneous tracking of two spacecraft in orbit about a distant planet by two widely separated Earth-based radio antennas provides more-accurate positioning information than can be obtained by tracking each spacecraft separately. A demonstration of this tracking technique, referred to as same-beam interferometry (SBI), is currently being done using the Magellan and Pioneer 12 orbiters at Venus. Signals from both spacecraft fall within the same beamwidth of the Deep Space Station antennas. The plane-of-sky position difference between spacecraft is precisely determined by doubly differenced phase measurements. This radio metric measurement naturally complements line-of-sight Doppler. Data were first collected from Magellan and Pioneer 12 on August 11–12, 1990, shortly after Magellan was inserted into Venus orbit. Data were subsequently acquired in February and April 1991, providing a total of 34 hours of same-beam radio metric observables. Same-beam radio metric residuals have been analyzed and compared with model measurement error predictions. The predicted error is dominated by solar plasma fluctuations. The rms of the residuals is less than predicted by about 25 percent for 5-min averages. The shape of the spectrum computed from residuals is consistent with that derived from a model of solar plasma fluctuations. This data type can greatly aid navigation of a second spacecraft when the first is well-known in its orbit.

I. Introduction

The Venus-relative positions of the Magellan (MGN) and Pioneer 12 (PVO) spacecraft are currently being determined independently by using Earth-based measurements of the radio signals emitted by each spacecraft. Simultaneous tracking of the two orbiters provides much stronger positioning information than is obtained by tracking just a single orbiter. The two spacecraft are so close angularly as seen from Earth that they may be observed in the same beamwidth of an Earth-based radio antenna. Radio metric data received at two Earth stations may be combined to provide an interferometric measurement of the plane-of-sky position difference between the two space-

craft. This measurement technique, called same-beam interferometry (SBI), is extremely precise due to double differencing of common errors along the four ray paths from the two spacecraft to the two ground stations. SBI measurements made at S-band (2.3 GHz) give plane-of-sky position change with an accuracy on the order of 10 m at Venus. A joint solution for the orbits of both spacecraft, combining Doppler and interferometric observables, provides up to an order of magnitude better accuracy than solutions for a single orbiter using only Doppler data.

A demonstration using the Magellan and Pioneer 12 orbiters is in progress to show the improvements to orbital accuracy that are provided by SBI, as compared with single-station Doppler. The first simultaneous data were acquired in August 1990, shortly after Magellan was inserted into Venus orbit, during the Magellan orbital checkout phase. SBI data were also acquired in February and April 1991. This article describes the data acquisition and presents an analysis of measurement system errors. An analysis of orbit solutions derived from these data will be presented in a following article.

SBI has been employed before, at the very beginning of the Pioneer 12 mission to Venus. Radio signals emitted from the four probes released by the orbiter were measured by SBI relative to the orbiter radio signal to determine the Venus wind speed and direction [1]. A similar determination was obtained from simultaneous interferometric measurements of the Vega spacecraft and the balloons that it dropped off at Venus [2]. Earlier, this technique was used to locate the Apollo 16 Lunar Rover relative to the Lunar Module [3] and to measure librations of the moon by using signals from the Apollo Lunar Surface Experiments Package (ALSEP) transmitters [4]. While these applications of SBI were of short duration and primarily for scientific purposes, NASA routinely and continuously tracks planetary orbiters. Obtaining telemetry and radio metric data simultaneously from two spacecraft at one station offers tremendous efficiency advantages. If, in addition, the two spacecraft are also simultaneously observed at a second, distant station during the mutual visibility period, then improved orbital accuracy results. Improved accuracy may increase science data return or reduce the total tracking time necessary to maintain a specified level of positional knowledge. The demonstration with Magellan and Pioneer 12 is the first step toward developing an operational capability for SBI data acquisition within NASA's Deep Space Network.

SBI system errors and the application of SBI to the positioning of planetary rovers, landers, and orbiters have been described previously [5–8]. When Doppler data are supplemented with SBI data, the expected improvement in orbital accuracy for two orbiters varies from a factor of two to a factor of ten, depending on data accuracy and strategy. The Space Exploration Initiative (SEI) proposes a series of missions to Mars, which will likely involve communications orbiters, mapping spacecraft in low orbits, rendezvous craft, stationary landers, and rovers. Early development of an SBI capability will enhance this mission set.

The interferometric measurement and its expected contribution to the orbit solution process are discussed in more detail in the next section. Analytic models for predicting SBI measurement errors are presented. The acquisition and processing of SBI data from the Magellan and Pioneer 12 orbiters are briefly discussed. SBI measurement residuals from the August 1990 and February 1991 data sets are then analyzed and compared with predicted errors.

II. Tracking Strategies and SBI

Doppler measures the line-of-sight range rate between a Deep Space Station and a spacecraft. An arc of Doppler data from a planetary orbiter provides a history of the change in range. Interferometric measurements naturally complement Doppler. The difference in arrival time of a signal at two stations provides a direct measure of the angle between the baseline vector joining the two stations and the direction to the radio source. This, in turn, provides a geometric measure of the plane-of-sky position of the radio source in the direction of the baseline projected onto the plane of the sky.

The Doppler observable is derived from measuring the phase of the spacecraft RF carrier signal. Both Magellan and Pioneer 12 are capable of transmitting at S-band (2.3 GHz) and X-band (8.4 GHz). Since phase can be measured to within a small fraction of a cycle, Doppler is precise enough to sense submillimeter-level changes in line-of-sight range. It is generally not possible to utilize the full precision of Doppler since neither media fluctuations nor spacecraft dynamics can be modeled to the millimeter level. The SBI observable (Fig. 1) is also derived from measuring the carrier phase. The SBI observable is the phase, first differenced between stations and then differenced between spacecraft. Errors in the line-of-sight phase measurements are greatly diminished by double differencing. The doubly differenced phase, $\Delta^2\phi$, is given approximately by

$$\lambda\ \Delta^2\phi = (B\sin\theta)\Delta\theta$$

where

$\lambda =$ the signal wavelength

$B =$ the length of the baseline

$\theta =$ the angle between the baseline and the direction to the spacecraft

$\Delta\theta =$ the difference in θ for the two spacecraft

The angular separation between spacecraft is measured with an accuracy given by the doubly differenced phase accuracy times the wavelength divided by the baseline length projected onto the plane of the sky. The plane-of-sky position accuracy (linear distance at the spacecraft) of an SBI measurement is equal to the Earth–spacecraft distance times the angular accuracy. For millicycle-phase accuracy, intercontinental baselines, and an Earth–spacecraft distance of one astronomical unit, the position accuracy is on the order of 1 m. The combination of complementary Doppler and SBI data allows for dramatic improvement in orbital accuracy as compared with Doppler alone. Actual improvement in accuracy will be sensitive to where in the orbit the data are acquired.

Because the SBI observable is obtained from the carrier phase, there is an integer cycle ambiguity in the SBI measurement. A priori knowledge of orbiter positions will generally be inadequate to resolve this ambiguity. Thus, SBI measures the change in plane-of-sky position, rather than absolute position, just as Doppler measures the change in line-of-sight position. An SBI bias, common to all data points in a continuous arc, must be estimated. If the error in the estimation of the bias is significantly less than one cycle, it may be possible to fix the integer cycle, thus strengthening the data set. All instrumental effects not common to both spacecraft signal chains must be calibrated if the bias is to be fixed.

The orbits of both spacecraft are estimated together when using SBI data. The Pioneer 12 orbit is less perturbed by Venus gravity-field mismodeling than is the short-period Magellan orbit. For example, given a good orbit for Pioneer 12, SBI data will geometrically transfer position accuracy to Magellan, independent of gravity mismodeling. On the other hand, if Magellan is tracked much more frequently than Pioneer 12, then the SBI data improve the Pioneer 12 orbit by tying it to the relatively well-known Magellan orbit. In general, the signature in SBI data will provide information to improve the orbits of both spacecraft.

Currently, for operational tracking of either Magellan or Pioneer 12, one Deep Space Station is in two-way communication with one spacecraft. The station transmits a signal that is coherently transponded by the spacecraft and received back at the transmitting station. The resulting measurement is referred to as two-way Doppler; orbit determination relies primarily upon this measurement. Orbit solutions for Magellan also make use of Doppler data received simultaneously at two stations and then differenced [9]. This data type, known either as narrowband VLBI [10], or more recently as differenced Doppler [11], has information content similar to that given by SBI, but is less accurate since measurement errors are not reduced by double differencing. For the SBI demonstration, Doppler data were acquired in the two-way mode from both Magellan and Pioneer 12, at separate stations. SBI data were acquired in an open-loop mode by using the Narrow Channel Bandwidth (NCB) VLBI System [12]. The NCB recordings were normally made on a noninterference basis at the Deep Space Stations scheduled for operational Magellan tracks. For some passes a separate station was scheduled for the purpose of recording with the NCB system. SBI data were acquired while both spacecraft were transmitting in the two-way mode, except for two passes when Magellan data were acquired in the one-way mode. The spacecraft onboard oscillator is the frequency reference for one-way Doppler and SBI. Because the received spacecraft signals are differenced between two stations, the SBI data accuracy does not depend on whether the tracking mode is one-way or two-way.

To realize advantages in efficiency by using SBI, it is of paramount importance to receive data from two or more spacecraft at a single station, with a second station to be used only during the baseline overlap periods. This mode of operation calls for replacing some or all of the two-way Doppler used for orbit determination with one-way Doppler so that multiple uplinks are not required, and it calls for simultaneous reception of telemetry from two spacecraft at one station. This is currently impractical for two reasons: (1) The oscillators on board the Magellan and Pioneer 12 spacecraft have insufficient stability to make one-way Doppler a viable alternative to two-way Doppler[1] and (2) the Deep Space Stations are configured to process only one telemetry signal stream at S-band and only one telemetry signal stream at X-band. In fact, dual support passes have been scheduled during which a single station receives Pioneer 12 telemetry at S-band and Magellan telemetry at X-band, but Doppler data are gen-

[1] D. Engelhardt, "Suitability of the MGN Onboard Auxiliary Oscillator for One-Way Doppler Data Generation," JPL Interoffice Memorandum 314.6-695 (internal document), Jet Propulsion Laboratory, Pasadena, California, July 28, 1986.

erated for only one spacecraft.[2] Future developments are expected to allow the DSN to fully realize the increased efficiency which SBI makes possible. Improvements to the stability of flight oscillators may enable orbit determination accuracy requirements to be met by using a combination of one-way Doppler and SBI data in place of two-way Doppler data [13]. The implementation of the Block V receiver in the DSN will enable simultaneous reception of Doppler and telemetry from at least two spacecraft at a single station at either S-band or X-band.[3]

III. Predicted SBI Measurement Errors

Measurement errors are predicted here for the SBI data obtained from MGN and PVO. Due to limited spacecraft battery capacity during data acquisition periods, Pioneer 12 was transmitting at S-band only, while Magellan was usually transmitting at both S-band and X-band. SBI data could be generated only at the S-band frequency, but the dual frequency downlink on Magellan was useful for characterizing charged particle delays. Measurements were compressed to either 2-sec, 20-sec, or 5-min averages over the 1-hr (typical) data arcs. Formulae for error prediction are developed that apply to arbitrary geometries and arbitrary frequencies. Solar plasma and instrumental phase shifts within the receiver are the two errors that are least perfectly canceled by double differencing, and generally they are limiting error sources for SBI measurements. These two error sources will be discussed in detail. For S-band measurements, the Earth's ionosphere is also a potentially significant error.

Distinction is made between (1) noiselike errors, which are random over a data arc and decrease with averaging time, and (2) errors that appear as slow drifts over a data arc. For this experiment, a constant measurement bias does not contribute an error, since an SBI data bias will be estimated for each data arc. Error predictions for SBI observables are given in picoseconds. One picosecond of time delay corresponds to 0.0023 cycle of phase at S-band, or to 0.0084 cycle of phase at X-band. Also, one picosecond of time delay corresponds to an angle of 37.5 prad over an 8000-km baseline, or to a transverse position of 8 m at 1.4 AU. Measurement errors are predicted for S-band SBI observables for the geometries of August 1990 and February 1991. For comparison, error predictions are also given for X-band SBI observables for the geometry of August 1990. The assumptions used in the error analysis are summarized in Tables 1–4. A histogram of error contributions is shown in Fig. 2. All errors are one-sigma.

At S-band, the signal measured for SBI is the carrier from PVO and the carrier signal transmitted from either the high-gain antenna (HGA) or medium-gain antenna from MGN. The S-band carrier signals are separated by about 4 MHz in frequency. At X-band, the signal measured for SBI is the carrier from PVO and the −16th harmonic of the high-rate telemetry subcarrier from Magellan. The −16th harmonic is chosen as the Magellan X-band reference signal because it has adequate power and is separated by only 0.1 MHz in frequency from the PVO X-band carrier, whereas the Magellan X-band carrier is offset by 15 MHz from the PVO X-band carrier. Magellan was transmitting at S-band from its medium-gain antenna on August 11–12, 1990, and was transmitting dual-frequency S- and X-band downlinks from its HGA in February and April 1991.

A. System Thermal Noise

The sampled radio band will contain both the spacecraft signal and also the ground-receiver generated noise, which is proportional to the system operating temperature. The system noise error depends on the ratio of received signal power to system noise power. The voltage signal-to-noise ratio (SNR) for one-bit sampling is given by

$$SNR_V = \sqrt{\frac{4}{\pi}\frac{P_{Tone}}{N_0}T_{obs}}$$

where P_{Tone} is the received spacecraft tone power, N_0 is the system noise power in a 1-Hz bandwidth, and T_{obs} is the averaging interval (in seconds). The SBI thermal noise error is given by

$$\epsilon_{SBI} = 10^{12}\sqrt{2}\frac{1}{2\pi}\sqrt{\frac{1}{SNR_{V1}^2 f_{RF1}^2} + \frac{1}{SNR_{V2}^2 f_{RF2}^2}} \text{ psec}$$

where SNR_{Vi} and f_{RFi} are, respectively, the SNR_V and radio frequency in hertz for spacecraft i. The leading $\sqrt{2}$ accounts for two stations. A link analysis showing the received signal power and resulting voltage SNR for 1-sec integration is given in Table 4. Recorder data are time-multiplexed between spacecraft, so that 1 sec of data is

[2] *Deep Space Network Test and Training Plan, Magellan/Pioneer-12 Simultaneous Support (MPSS)*, JPL 870-176 (internal document), Jet Propulsion Laboratory, Pasadena, California, August 20, 1990.

[3] *Deep Space Communications Complex, Block V Receiver Implementation Task, Volume 5: Functional Requirements*, JPL 803-112 (internal document), Jet Propulsion Laboratory, Pasadena, California, May 1, 1991.

recorded for each spacecraft in a 2-sec interval. The SNR_V for 20-sec averages is $\sqrt{10} \times SNR_{V,1sec}$, and the SNR_V for 5-min averages is $\sqrt{150} \times SNR_{V,1sec}$. System noise is a random error source. Though not decreased by station differencing or spacecraft differencing, system noise is reduced as averaging time increases.

B. Instrumental Phase Shifts

The instrumental phase response of the receiver system is characterized predominantly as a group delay: The instrumental phase shift is a linear function of the frequency of the received signal. Deviations from linearity due to dispersion take two forms: a curvature that slowly varies with signal frequency and a much more rapidly varying "ripple." SBI measurements are affected in a systematic way as the Doppler shift causes the received signal frequency to sweep across the passband. Phase shifts due to instrumental group delays and clock offsets are referred to as linear systematic; phase shifts due to bandpass curvature are referred to as nonlinear systematic; and shifts due to the deviation of the system phase response from a smooth phase response are referred to as phase ripple.

1. Linear Systematic. The time-dependent station-differenced phase shift $\phi_I(t)$ for a single spacecraft due to instrumental group delays and station clock epoch offsets can be shown to be[4]

$$\phi_I(t) = f_{RF}\left(\nu(t)\tau_I + \dot{\rho}(t)\delta\tau_{clock} - \delta\tau_{clock}\right) + \Delta\phi_h \text{ cycles}$$

where f_{RF} is the transmitter frequency (in hertz); $\nu(t)$ is the interferometer fringe frequency (in sec/sec); $\dot{\rho}(t)$ is the line-of-sight range rate to Station 1 (in sec/sec); τ_I is the instrumental group delay at Station 2 (in seconds); $\delta\tau_{clock}$ is the error in modeling the clock epoch offset between stations (in seconds); and $\Delta\phi_h$ is a constant instrumental phase shift (in cycles). Note that $\nu(t)$ is the line-of-sight range rate differenced between stations. The term $\dot{\rho}(t)$ refers to Station 1, and the term τ_I refers to Station 2, due to the convention that was used to select a clock reference point. The phase shift $\phi_I(t)$ causes an SBI error because the model for spacecraft-received phase does not account for certain instrumental delays and, of course, for an unknown clock offset. A constant phase shift is absorbed by estimating an SBI data bias. SBI errors will be induced by a change in ϕ_I over the data arc, which is not common to both sources. The change in ϕ_I over a data arc due to the change in ν and $\dot{\rho}$ is

$$\delta\phi_I = f_{RF}\left(\delta\nu\tau_I + \delta\dot{\rho}\delta\tau_{clock}\right) \tag{1}$$

The interferometer fringe frequency ν, approximately given by the Earth rotation rate times the baseline length divided by the speed of light, is almost independent of spacecraft velocity for a distant spacecraft. The change in ν over a pass may be $\delta\nu = 0.3$ μsec/sec. The instrumental group delay τ_I is about 25 μsec. But $\delta\nu$ is almost the same for two spacecraft at Venus, the difference being on the order of 1 nsec/sec. This makes the first term in Eq. (1) an insignificant SBI error. The change in line-of-sight range rate $\delta\dot{\rho}$ will be distinct for each spacecraft, unless they share an orbit (e.g., lander and rover). For SBI data arcs acquired in August 1990, the maximum change in $\delta\dot{\rho}$ occurred for Magellan and was 22 μsec/sec. A clocklike offset between stations can be measured with subnanosecond precision by making interferometric observations of natural radio sources. However, the term $\delta\tau_{clock}$ above refers to the error in knowledge of time tags. Currently this knowledge is on the order of 0.1 μsec. Ambiguities in instrumental calibrations have prevented absolute time-tag synchronization at the precision of the measurements. This is not a fundamental limitation; nanosecond-level synchronization is entirely feasible [14]. The second term in Eq. (1) is one of the largest SBI errors; improved synchronization is, in fact, required to reduce this error source. The SBI error due to linear systematic effects is given by

$$\epsilon_{SBI} = 10^{12}\delta\dot{\rho}\ \delta\tau_{clock} \text{ psec}$$

This error changes slowly over a pass, as $\dot{\rho}$ changes.

2. Nonlinear Systematic. The phase response of the baseband filters has a known systematic curvature. The curvature is almost the same at each station. The received baseband frequencies will, in general, differ at each station due to the rotation of the Earth, so the station-differenced phase shift will not be zero. The phase shift will change as the narrowband signal sweeps across the passband. To estimate the size of this effect, suppose that the curvature is quadratic over $2F$ kHz with a peak-to-peak phase nonlinearity of $2A$ deg. Suppose that the baseband frequencies at the two stations are separated by δf_{bb} kHz. Then, the maximum station-differenced phase shift as the received signal sweeps from $-F$ to $+F$ kHz at Station 1 is

$$\delta\phi_c \approx \pm \frac{4A\delta f_{bb}}{F} \text{ deg}$$

In August 1990, the Magellan received frequency changed by about 50 kHz over a 1-hr data arc, while the

[4] J. S. Border, "Analysis of Clock and Instrumental Group Delays in ΔVLBI Observables," JPL Interoffice Memorandum 335.1-90-002 (internal document), Jet Propulsion Laboratory, Pasadena, California, January 5, 1990.

PVO received frequency changed by less than 3 kHz. The peak-to-peak nonlinear phase response over 50 kHz is estimated to be 2 deg for the open-loop receiver system used [15]. The offset in baseband frequencies between stations was 4 kHz for data acquired in August 1990. This gives a phase shift of $\delta\phi_c = 0.64$ deg.

The SBI error is given by

$$\epsilon_{SBI} = 10^{12} \frac{\delta\phi_c/360 \text{ deg}}{f_{RF}} \text{ psec}$$

This error varies slowly, as the line-of-sight range rate varies, and does not cancel between spacecraft. The error can be made smaller by either modeling the curvature of the passband or by offsetting station mixing frequencies so that baseband frequencies will be nearly equal. For data acquisitions in February and April 1991, station mixing frequencies were offset, virtually eliminating the error due to bandpass curvature at baseband. There also is an error of this form due to curvature at RF and IF, which is not eliminated by offsetting station mixing frequencies, though the magnitude of this curvature is estimated to be smaller than the curvature at baseband by a factor of ten.

3. Phase Ripple. The phase ripple ϵ_ϕ for the open-loop system used to record the SBI data is estimated to be 0.5 deg [15]. Most of the ripple comes from the baseband filter, though RF and IF components also contribute. Variations of ± 0.5 deg away from the smooth systematic curvature of the bandpass occur over scales of a few kilohertz. Thus, this error is generally independent for each spacecraft and each station, since received frequencies are not equal. The SBI error is given by

$$\epsilon_{SBI} = 10^{12} \frac{2\epsilon_\phi/360 \text{ deg}}{f_{RF}} \text{ psec}$$

Received frequencies from Venus orbiters may change by a few kilohertz in 5 min, or by much less, so this error is random or systematic, depending on the orbital geometry. For the MGN–PVO data set of August 1990, the error component due to Magellan is random, while the error component due to PVO is slowly varying. For a data arc that includes the time of PVO periapsis, the error component due to PVO is random rather than systematic.

C. Transmitter Frequency Offset

Clock offsets and instabilities at both transmitters and receivers are nearly eliminated by differencing. But the transmitter frequency is used to convert between calculated geometric time delays and observed phase delays. An unknown offset δf_T (in hertz) between the transmitter frequencies of two spacecraft will cause an SBI error of

$$\epsilon_{SBI} = 10^{12} \tau \frac{\delta f_T}{f_{RF}} \text{ psec}$$

where τ (in seconds) is the interferometric delay. For two-way signals, where the spacecraft is transponding a signal uplinked from a ground station, the offset $\delta f_T / f_{RF}$ is a measure of clock-rate synchronization between the two stations that are uplinking to the two spacecraft. The DSN station clock rates are generally synchronized to 10^{-13} sec/sec, though a few stations have independent clocks that may have unknown rate offsets as large as 10^{-12} sec/sec. The interferometric delay may range over -0.02 to $+0.02$ sec. This error source is insignificant for two-way transmissions, such as were used for nearly all the Magellan and Pioneer 12 measurements. For one-way transmissions, the spacecraft onboard oscillator frequency must be estimated to the 0.1-Hz level in order to reduce the size of this error below one picosecond.

D. Baseline

Baseline errors include uncertainties in station location, Earth orientation, and frame tie. The DSN Earth-fixed baseline components are known to 5 cm. Calibrations for UT1–UTC, polar motion, and nutation tweaks are available about 2 weeks after the measurement epoch that provides Earth orientation accuracy of 5 cm per component in the radio frame. Real-time predictions are currently at the 30-cm level, but may improve to 5 cm over the next few years as Global Positioning System (GPS) satellite measurements are incorporated into Earth orientation solutions [16,17]. Since the positions of the spacecraft being tracked are specified relative to Venus, the orientations of the baselines in the planetary frame are required. Knowledge of the orientation offset between the radio frame and the planetary frame is estimated to be 25 nrad [18]. This causes a baseline error of 20 cm per component. The rss baseline error (for data processed 2 weeks after real time) is 21.2 cm per component. The SBI error is given by

$$\epsilon_{SBI} = \frac{10^{12}}{c} \epsilon_{BL} \, \Delta\theta \text{ psec}$$

where ϵ_{BL} is the baseline component error (in centimeters), $\Delta\theta$ is the angular separation of the two spacecraft (in radians), and c is the speed of light (cm/sec). This error term is slowly varying over a pass.

E. Troposphere

Signal path delay through the troposphere is a function of the zenith tropospheric delay and source elevation angle. The zenith delay is computed from surface meteorology data, mapped to the line of sight, and applied as a calibration for each source. The calibration error depends on the uncertainty in the determination of zenith delay and the differential elevation angle between sources. Uncertainty in the static component of the zenith delay is dominated by the uncertainty in determining the wet component. Spatial fluctuations in water vapor content also affect SBI observables.

1. Zenith Bias. At a single station, the error due to a zenith bias is given by

$$\epsilon_{SBI} = \frac{10^{12}}{c} \frac{\rho_{zt} \cos\gamma}{\sin^2\gamma} \delta\gamma \quad \text{psec}$$

where ρ_{zt} is the uncertainty in the measurement of zenith delay (in centimeters), c is the speed of light (cm/sec), γ is the source elevation angle, and $\delta\gamma$ is the differential elevation angle between sources (in radians). This error will be independent at each station and will vary slowly over a pass. It is calculated for the MGN–PVO data set from the parameters in Tables 2 and 3.

2. Fluctuations. Two ray paths from a single station, separated by $\Delta\theta$ rad, may be thought of as having a spatial separation of $3h_t\Delta\theta$ in the tropospheric shell, where h_t is the effective wet tropospheric height ($h_t \approx$ 1 km) and 3 is the mapping to the typical elevation angle of 20 deg. An estimate for the effect of spatial fluctuations on two ray paths separated by this distance may be derived from the structure function of tropospheric delay developed by Treuhaft and Lanyi [19]. Fluctuations are described by Kolmogorov turbulence. For small angular separations ($\Delta\theta \leq 1$ mrad), expressed as a function of the angle $\Delta\theta$ (in radians), the SBI error is given by

$$\epsilon_{SBI} = \sqrt{2}\ 48\Delta\theta^{5/6} \text{ psec}$$

$$\text{decorrelation time} = (3h_t\Delta\theta)/v_t \text{ sec}$$

where $v_t \approx 0.008$ km/sec is the tropospheric wind speed and the leading $\sqrt{2}$ accounts for two stations. For the August 1990 MGN–PVO data set, with $\Delta\theta = 0.3$ mrad, the SBI error is 0.08 psec with a decorrelation time of 0.11 sec. This error is insignificant.

F. Ionosphere

The ionosphere is a dispersive medium; path delay scales as the inverse of frequency squared. Charged particle effects can be eliminated by observing at two radio frequencies, such as S- and X-band. For single-frequency data, calibrations are applied based on measurements of the total electron content (TEC) along the line of sight from each Deep Space Station to one or more beacon satellites. A mapping function, which depends on elevation angle and on the arc length in the ionospheric shell between the Earth–sun line and the source ray path, is used to calculate calibrations for each source. Systematic errors are caused by uncertainty in the measured TEC to the beacon satellite, by mapping error, and by a difference in radio frequency between the two observed sources. Spatial fluctuations in TEC also affect SBI observables.

1. Zenith Bias. For a single source, the total ionospheric delay can be written as

$$\tau_{ION} = 1340 \frac{f\ TEC_z}{f_{RF}^2} \quad \text{psec}$$

where TEC_z is the zenith delay in TEC units (10^{16} el/m^2), f is the mapping function from zenith to line of sight, and f_{RF} is the radio frequency in gigahertz. The differential error, after calibration, for two sources observed at one station is then given by

$$\epsilon_{SBI} = 1340 \frac{\rho_{zi}}{f_{RF}^2} \left(\frac{\partial f}{\partial \theta} \Delta\theta + 2f \frac{\delta f_{RF}}{f_{RF}} \right) \quad \text{psec} \qquad (2)$$

where ρ_{zi} is the error in the zenith delay measurement (in TEC units), $\partial f/\partial\theta$ is the spatial derivative[5] of the mapping function, and δf_{RF} (in gigahertz) is the difference in frequency between the two observed sources. Zenith delay calibrations were obtained from Faraday rotation measurements of geostationary satellite beacons and from dual-frequency group delay measurements of the available GPS satellites. The zenith error ρ_{zi} is estimated to be 5 TEC units. To estimate $\partial f/\partial\theta$ for the MGN–PVO data set, calibrations mapped to line of sight were examined for the full Venus visibility window for each station complex. The maximum change in the mapping function per unit change in angle was found to be $\partial f/\partial\theta = 6.9$ rad^{-1}. For

[5] The mapping function f depends on the two-dimensional angle that defines the ray path, and it depends on diurnal variations in zenith TEC. Here, the zenith error ρ_{zi} is considered to be constant and $\partial f/\partial\theta$ is computed as the maximum (over all directions) change in mapped calibration per unit angle.

$\Delta\theta = 0.3$ mrad, the first term in Eq. (2) is 2.6 psec. This term slowly varies over a pass, as the zenith measurement error and the geometry change. For a typical mapping of $f = 3$, the second term in Eq. (2) is 13.2 psec. But this is the total effect; a constant offset is absorbed by estimation of an SBI data bias. The SBI data are only sensitive to a change in the delay due to this term. The mapped calibration changed by at most 25 TEC units over a MGN–PVO pass. The change in the calibration error is expected to be 10 percent of this. Substituting 2.5 TEC units for $f\rho_{zi}$ in the second term gives an SBI error of 2.2 psec. The total systematic error will not be increased by $\sqrt{2}$ since neither the spatial derivative of the mapping function nor the drift in calibration error is expected to be large at both complexes concurrently.

Ionospheric calibration uncertainty is a potentially significant error source for S-band SBI measurements. This source of error is expected to be reduced by a factor of 2 to 5 when dual-frequency GPS group-delay measurements become available from a full GPS constellation for generation of ionospheric calibrations. Also, the component of error dependent on frequency difference between sources can be reduced if even one source transmits dual-frequency S–X signals. The dual-frequency transmissions allow precise measure of the change in TEC along the line of sight. The Magellan spacecraft transmitted dual-frequency S–X signals during the February and April 1991 SBI measurement sessions. The dual-frequency data were used to check the externally supplied ionosphere calibrations. For this data set, the observables were changed by an insignificant amount when the Faraday/GPS calibrations were adjusted so that the change in TEC along the line of sight was as measured by the Magellan S–X data.

2. Fluctuations. Temporal fluctuations in the ionospheric delay rate, after removal of a nominal calibration, have been observed to be about 3.8×10^{-14} sec/sec for X-band signals, for daytime low-elevation observations, and for averaging intervals from 60 to 6000 sec.[6] An estimate for SBI errors due to spatial fluctuations will be derived from this result. The angular separation $\Delta\theta$ (in radians) between ray paths corresponds to a spatial separation d (in kilometers) in the ionospheric shell and to a temporal separation T (in seconds) between measurements through the relations

$$d \approx T v_i \approx 3 h_i \Delta\theta$$

where $v_i \approx 0.1$ km/sec is the ionospheric wind speed, 3 is a typical elevation scale factor, and $h_i \approx 350$ km is the effective height of the ionosphere. Spatial fluctuations in delay, for angles from 0.006 to 0.6 rad, appear to scale linearly with the angle, since delay rate variations are flat over corresponding time intervals. It may be optimistic to assume that the angular dependence remains linear for very small angles. Instead, Kolmogorov turbulence will be assumed. Thus, the error is of the form $k\Delta\theta^{5/6}$ for small angles. The constant k is defined by making this expression predict an error for $\Delta\theta = 0.00571$ rad, which is consistent with the corresponding observed temporal variations for a time offset of 60 sec. The resulting SBI error is

$$\epsilon_{SBI} = \sqrt{2}\frac{11700}{f_{RF}^2}\Delta\theta^{5/6} \quad \text{psec}$$

$$\text{decorrelation time} = (3h_i\Delta\theta)/v_i \quad \text{sec}$$

where f_{RF} is the observing frequency in gigahertz and $\sqrt{2}$ accounts for two stations. For the August 1990 MGN–PVO data set, with $\Delta\theta = 0.3$ mrad, the SBI error is 3.6 psec with a decorrelation time of 3.15 sec.

G. Solar Plasma

To model solar plasma–induced fluctuations on radio signals transmitted by interplanetary spacecraft, the plasma is imagined to be confined to a thin screen passing through the center of the sun and perpendicular to the line connecting the spacecraft and the Earth. Define a random function, $\phi(x)$, which represents the phase fluctuation induced on a radio signal as it penetrates the plasma screen at a distance x from the center of the sun. Then the quantity $\phi(b+x) - \phi(x)$ represents the differential phase fluctuation induced on two signals that are separated by a distance b when passing through the plasma screen. For an interferometric observation, b is the length of the projection of the baseline onto the plasma screen. For an observation of a spacecraft at Venus from a DSN baseline, b is typically 4000 km.

To determine the plasma-induced phase error on interferometric measurements, the spatial structure function of phase, $D(b)$, is computed. It is defined as: $D(b) \equiv \left\langle (\phi(b+x) - \phi(x))^2 \right\rangle$. Here, brackets denote an ensemble average. The value $D(b)$ may be viewed as representing the phase variance of a station-differenced phase measurement. The power spectrum of electron density fluctuations, which has been determined experimentally [20], can be used to calculate a formula for $D(b)$ [21]

[6] A. J. Mannucci, "Temporal Statistics of the Ionosphere," JPL Interoffice Memorandum 335.1-90-056 (internal document), Jet Propulsion Laboratory, Pasadena, California, October 25, 1990.

$$D(b) = \frac{2.5 \times 10^{-4}}{(f_{RF})^2} \times (b/v_{sw})^{1.65}$$

$$\times (\sin(SEP))^{-2.45} \quad \text{cycles}^2 \qquad (3)$$

In this expression, f_{RF} is the signal radio frequency in gigahertz, SEP is the sun-Earth-probe angle, and v_{sw} is the velocity of the solar wind (typically 400 km/sec).

Knowledge of the structure function enables calculation of the temporal correlations between plasma-induced errors on interferometric measurements. First note that because of the dynamics of the solar wind, the plasma-induced phase fluctuation, ϕ, is actually a function of both space and time, $\phi = \overline{\phi}(x,t)$. If, however, it is assumed that the plasma turbulence consists of fixed structures that maintain their shape as they travel radially outward from the sun at velocity v_{sw}, then ϕ may be written as a function of a single variable $\overline{\phi}(x,t) = \phi(x - v_{sw}t)$.

Let $\Delta\Phi(b,T_i) \equiv \overline{\phi}(b+x,t_i) - \overline{\phi}(x,t_i)$ and $\Delta\Phi(b,T_j) \equiv \overline{\phi}(b+x,t_j) - \overline{\phi}(x,t_j)$ be the station-differenced phase at Earth receive times T_i and T_j, along a baseline whose projection onto the plasma screen has length b. Here, $t_i = T_i$ − [light travel time from plasma screen to Earth], and $t_j = T_j$−[light travel time from plasma screen to Earth]. (The slight difference in signal arrival time at the two stations is ignored here.)

Then, the temporal covariance is computed as

$$\begin{aligned}\langle \Delta\Phi(b,T_i)\,\Delta\Phi(b,T_j)\rangle &= \langle (\overline{\phi}(b+x,t_i) - \overline{\phi}(x,t_i)) \\ &\quad \times (\overline{\phi}(b+x,t_j) - \overline{\phi}(x,t_j))\rangle \\ &= \langle \overline{\phi}(b+x,t_i)\,\overline{\phi}(b+x,t_j)\rangle \\ &\quad - \langle \overline{\phi}(b+x,t_i)\,\overline{\phi}(x,t_j)\rangle \\ &\quad - \langle \overline{\phi}(b+x,t_j)\,\overline{\phi}(x,t_i)\rangle \\ &\quad + \langle \overline{\phi}(x,t_i)\,\overline{\phi}(x,t_j)\rangle\end{aligned}$$

Assuming that ϕ is stationary,

$$\begin{aligned}\langle \overline{\phi}(x,t)\overline{\phi}(y,t')\rangle &= \langle \phi(x - v_{sw}t)\,\phi(y - v_{sw}t')\rangle \\ &= \langle \phi(x - y - v_{sw}(t-t'))\,\phi(0)\rangle\end{aligned}$$

and

$$D(\rho) = \left\langle (\phi(\rho + x) - \phi(x))^2 \right\rangle = 2\left\{\langle \phi^2\rangle - \langle \phi(\rho)\phi(0)\rangle\right\}$$

Applying the above two equations yields

$$\begin{aligned}\langle \Delta\Phi(b,T_i)\,\Delta\Phi(b,T_j)\rangle &= \langle \phi^2\rangle - 1/2D(v_{sw}(t_j - t_i)) \\ &\quad - \langle \phi^2\rangle + 1/2D(b - v_{sw}(t_j - t_i)) \\ &\quad - \langle \phi^2\rangle + 1/2D(b + v_{sw}(t_j - t_i)) \\ &\quad + \langle \phi^2\rangle - 1/2D(v_{sw}(t_j - t_i)) \\ &= 1/2D(b - v_{sw}(t_j - t_i)) \\ &\quad + 1/2D(b + v_{sw}(t_j - t_i)) \\ &\quad - D(v_{sw}(t_j - t_i))\end{aligned}$$

Since D can be computed by using Eq. (3) above, this expression for the temporal covariance between station-differenced phase measurements can be used to estimate the plasma-induced error on an interferometric observable that is derived from a time average of "instantaneous" measurements. As an example, consider a spacecraft at Venus on August 11, 1990, transmitting an S-band signal that is simultaneously received at Goldstone and Canberra. The SEP angle is 21 deg, and the projection of the baseline onto the plasma screen is 4000 km. The above model for the solar plasma yields a plasma-induced station-differenced delay error of 40 psec over 5 min.

The SBI observable is formed from doubly differenced phase observables. For spacecraft whose separation is less than 1 deg, double differencing of phase observables can result in significant cancellation of the plasma-induced error. Let $\Delta^2\Phi(S,b,T_j)$ be the doubly differenced phase at time T_j. Here S is the separation (on the plasma screen) between the signals transmitted by the two spacecraft (Fig. 3). Then, the instantaneous phase variance is

$$\begin{aligned}\Delta^2\Phi(S,b,T_j) &\equiv \{\Delta\Phi(b,T_j)\}_{S/C1} - \{\Delta\Phi(b,T_j)\}_{S/C2} \\ &= \{\overline{\phi}(S+b+x,t_i) - \overline{\phi}(S+x,t_i)\} \\ &\quad - \{\overline{\phi}(b+x,t_i) - \overline{\phi}(x,t_i)\}\end{aligned}$$

The covariance between doubly differenced phase measurements, $\langle \Delta^2\Phi(S,b,T_i)\,\Delta^2\Phi(S,b,T_j)\rangle$, can be com-

puted by first applying the substitution above and then proceeding in an analogous fashion to the calculation for singly differenced phase measurements. The final result is

$$\begin{aligned}\left\langle \Delta^2\Phi\left(S,b,T_i\right)\Delta^2\Phi\left(S,b,T_j\right)\right\rangle = &-2D\left(v_{sw}\left(t_j-t_i\right)\right)+D\left(b+v_{sw}\left(t_j-t_i\right)\right)+D\left(S+v_{sw}\left(t_j-t_i\right)\right)\\ &+D\left(-b+v_{sw}\left(t_j-t_i\right)\right)+D\left(-S+v_{sw}\left(t_j-t_i\right)\right)\\ &-1/2D\left(b+S+v_{sw}\left(t_j-t_i\right)\right)-1/2D\left(S-b+v_{sw}\left(t_j-t_i\right)\right)\\ &-1/2D\left(b-S+v_{sw}\left(t_j-t_i\right)\right)-1/2D\left(-b-S+v_{sw}\left(t_j-t_i\right)\right)\end{aligned}$$

D can be computed by using Eq. (3) above, so this expression for the temporal covariance between doubly differenced phase measurements can be used to estimate the plasma-induced error on an SBI observation.

In the August 1990 SBI experiment, the SEP angle was 21.3 deg. The baseline projection onto the plasma screen, b, was about 3300 km for Goldstone–Madrid and 4000 km for Goldstone–Canberra; the projection of the spacecraft separation, S, was about 40,000 km during the Goldstone–Madrid observations and 30,000 km during the Goldstone–Canberra observations. Using the above model for the solar plasma, the plasma-induced SBI error for a 5-min average is 13 psec at S-band for each baseline. This is substantially smaller than the 40-psec plasma-induced delay error for a single spacecraft interferometric observable; because Magellan and PVO are angularly close (separation $\approx$ 0.3 mrad), plasma-induced phase advances on signals transmitted by each spacecraft are highly correlated. The predicted SBI error for a 2-sec average is 81 psec, while the error for a 20-sec average is 64 psec. Errors have high temporal correlation for averaging times less than 100 sec.

This calculation of the covariance between doubly differenced phase measurements assumes that the two spacecraft transmit signals at exactly the same frequency; Magellan and PVO transmit signals at 2297 GHz and 2293 GHz, respectively. Since (1) plasma-induced phase advance is inversely proportional to frequency; (2) the spacecraft frequencies differ by only 0.2 percent; and (3) the predicted doubly differenced phase error is only about a factor of three less than the singly differenced phase error, the temporal covariance of doubly differenced phase measurements differs from the above estimate by less than one percent.

It should be noted that the separations S and b typically have components that are not in the solar radial direction. It is expected that the error for such a measurement is comparable with the error calculated via the simple model above. Large-scale turbulence (>40,000 km or, equivalently, hundreds of seconds) is still common to all four signal paths; small-scale turbulence (less than a few thousand kilometers or, equivalently, several seconds) is not common to any of the signal paths, regardless of the orientation of S and b. Thus, for averaging times of 2 sec or 5 min, the predicted plasma-induced error on the SBI measurement should not depend strongly on the orientation of S and b.

SBI observations of two spacecraft with yet smaller angular separation would benefit from even greater cancellation of the solar plasma error. SEI encompasses an extensive series of missions to Mars beginning in the late 1990s. Two spacecraft separated by thousands of kilometers on the Martian surface would have an angular separation on the order of 5–10 μrad as viewed from Earth; when Mars is at a 20-deg SEP angle, the plasma-induced phase error for a 5-min S-band SBI observation of two landed spacecraft is less than 2.2 psec.

Solar plasma turbulence can vary substantially from day to day, potentially resulting in an order of magnitude variation in plasma-induced phase error at a given SEP angle [20].

H. Root-Sum-Square Error

The total predicted measurement error is computed as the rss of individual error terms. It is evident from Fig. 2 that solar plasma fluctuations dominate S-band SBI errors for the geometry of August 1990. This error term is reduced for the geometry of February 1991, due to the reduced angular separation between the two spacecraft as seen from Earth. Errors due to station instrumentation and the Earth's ionosphere are comparable to the solar

plasma error for the geometry of February 1991. The predicted one-sigma rss error for the S-band SBI measurements acquired in February 1991 from Magellan and PVO is, for averaging intervals of 2 sec, 20 sec, and 5 min, equal to 56 psec, 30 psec, and 4.8 psec, respectively. The plane-of-sky separation between the two spacecraft is thus measured with a precision of 41 m, after a 5-min integration. All observables in a continuous data arc will have a common bias, due to the integer cycle ambiguity in the measurement of radio signal phase.

IV. Data Acquisition and Processing

SBI data may be acquired during the overlap periods when Venus is visible from either the Goldstone–Madrid baseline or the Goldstone–Canberra baseline, provided that both Magellan and Pioneer 12 are transmitting. Neither spacecraft transmits continuously, however. Magellan, which has an orbital period of 3.25 hr, transmits to Earth for approximately 2 hr of each revolution. Data are unavailable when Magellan is making radar measurements of the Venus surface or performing a star calibration. Pioneer 12 transmission time is limited by the amount of power available at the spacecraft, which has been decreasing during the last few years. Daily transmission time has typically been in the range of 4 to 12 hr since August 1990. SBI data were scheduled when both Magellan and Pioneer 12 were expected to be transmitting during baseline overlaps.

Doppler data were acquired whenever possible. During each day, tracking shifts from the DSN complex at Madrid, Spain; to Goldstone, California; to Canberra, Australia. Reference orbits were generated separately for each spacecraft by using the two-way Doppler.

A total of 33.5 hr of SBI data were acquired from Magellan and Pioneer 12; the amount of data acquired during each experiment set for each baseline is listed in Table 5. Figure 4 shows the Venus-centered orbits of the two spacecraft for the geometry of August 1990, projected onto the plane of the sky, and indicates where in the orbits SBI data were acquired. Pioneer 12 was near apoapsis for all SBI data acquisitions in August 1990. During February and April 1991, Pioneer 12 was near periapsis during the Goldstone–Canberra overlap.

The NCB VLBI System was used to make an open-loop recording (1-bit samples) of the received signal voltage in 250-kHz channels that contained the S-band carrier signals from each spacecraft. The Magellan X-band carrier signal was also recorded in the February and April 1991 experiments. The signal phase was extracted at 1-sec intervals by digitally mixing a model of the received phase with the recorded signal voltages. For each spacecraft, the phase was differenced between stations, then further compressed to either 20-sec or 5-min averages. Residuals were obtained by removing a model based on the reference trajectories and by applying calibrations for tropospheric and ionospheric delays. Tropospheric calibrations were based on surface meteorological data, and ionospheric calibrations were based on either Faraday rotation measurements or dual-frequency GPS satellite measurements. SBI residuals were then obtained by differencing between spacecraft. Using two-way Doppler and SBI, a simultaneous solution for the orbits of both spacecraft was then generated. For the purpose of examining measurement errors, residuals were recomputed with respect to the new spacecraft orbits.

V. Analysis of Measurement Residuals

The magnitude of measurement errors and the characterization of correlations among measurements are important inputs to the orbit determination process. SBI residuals are examined here in an attempt to validate the error budget. Since the spacecraft orbits were fit to the SBI data as well as to the longer Doppler data arcs, it is possible that systematic SBI measurement errors have been absorbed into the spacecraft orbits. Checks of orbit consistency and orbit prediction will be necessary to resolve this issue. Here, examination is restricted to residuals of individual data arcs.

Residuals of 2-sec averages are displayed in Fig. 5 for the longest contiguous data arc acquired in August 1990. The geocentric angular separation of the two spacecraft is also shown. The predicted one-sigma error is 82 psec for 2-sec averages. The rms of the residuals is less than the prediction by about a factor of three at this time scale. When data are further compressed to 5-min averages, the rms is less than the predicted error of 14 psec by about 25 percent.

Residuals of 20-sec averages are shown in Fig. 6 for SBI data acquired on the Goldstone–Canberra baseline on February 17, 1991. A dramatic drop in the point-to-point scatter occurs where the angular spacecraft separation (also shown in Fig. 6) reduces from 100 to 30 μrad. This is believed to be the result of a more complete cancellation of solar plasma effects. Angular spacecraft separations below 100 μrad did not occur during SBI data recordings in August 1990.

Figure 7 shows residuals of 20-sec averages for SBI data acquired on the Goldstone–Canberra baseline on February

20, 1991. The variation in angular separation over this data arc is comparable to the variation over the data arc displayed in Fig. 6, yet the apparent reduction in point-to-point scatter is much less dramatic at the point of closest angular approach. This may be due to temporal variations in solar wind intensity or to geometric factors not accounted for in the solar plasma error model developed here. But, for both the February 17 and the February 20 data arcs, the rms of residuals for 20-sec averages is less than that predicted by the error budget. The rms for February 17 is 29 psec; the rms for February 20 is 18 psec; while the error budget prediction (assuming 90-μrad angular separation) is 30 psec.

According to the measurement error budget, solar plasma is the dominant error source at S-band frequencies for most geometries. Without dual-band measurements, it is difficult to separate dispersive and nondispersive errors in the residual phase; one method of determining whether the measurements are consistent with the error budget is to examine the power spectrum of the doubly differenced residual phase to see whether it conforms to the behavior expected of the solar plasma. Radio scattering experiments with the Pioneer and Viking spacecraft [20,22] have established that the one-dimensional power spectrum of solar plasma–induced phase scintillations follows a power law of the form $P_\phi(f)$ proportional to $f^{-2.65}$. Since the SBI observable is formed by doubly differencing four line-of-sight phase measurements, the form of the spectrum for the SBI observable will be somewhat modified; differencing the signals acts as a crude high-pass filter.

The function $\phi(x - v_{sw}t)$ has been defined in Section III.G as representing the plasma-induced phase advance on an individual signal traversing the plasma screen at a distance x from the sun at time t. Define $\varphi_x(t) = \phi(x - v_{sw}t)$. Then $\varphi_x(t)$ represents the temporal phase fluctuations induced by the plasma at a distance x from the sun. The power spectrum of the temporal phase fluctuations is the Fourier transform of the autocorrelation of φ_x. The power spectrum is of the form $Kf^{-2.65}$, where the value of the constant K depends on the distance x, or equivalently, the SEP angle. For a spacecraft at a 20-deg SEP angle transmitting a 2.3-GHz signal, $P_{\varphi x}(f) = 3.9 \times 10^{-6} f^{-2.65}$ cycles^2/Hz [20]. To represent a doubly differenced phase measurement, define a new function, $\xi_x(t) = \varphi_x(t+\tau_S+\tau_b) - \varphi_x(t+\tau_S) - \varphi_x(t+\tau_b) + \varphi_x(t)$, where τ_b is the length of the baseline projection on the plasma screen, b, divided by the solar wind velocity, and τ_S is the projection of the spacecraft separation on the plasma screen, S, divided by the solar wind velocity. The power spectrum of ξ_x can be derived by Fourier transforming the autocorrelation of ξ_x. The result is given by the following expression:

$$\begin{aligned} P\xi_x(f) &= 2P_{\varphi x}(f)[2 - 2\cos(2\pi\tau_b f) \\ &\quad - 2\cos(2\pi\tau_S f) + \cos(2\pi(\tau_b + \tau_S)f) \\ &\quad + \cos(2\pi(\tau_b - \tau_S)f)] \end{aligned} \tag{4}$$

Note that when f is small, as compared with $1/\tau_b$ and $1/\tau_S$, a Taylor series expansion of the cosines in the above equation shows that $P_{\xi x}(f)$ is proportional to $f^{+1.35}$. For higher frequencies, the power spectrum follows a power law of the form $f^{-2.65}$, which is modulated by cosines.

For the SBI experiment in August 1990, τ_b and τ_S were typically 10 sec and 75 sec (here a solar wind velocity of $v_{sw} = 400$ km/sec is assumed). Using these values, Eq. (4) is plotted in Fig. 8 with the power spectrum of SBI residuals from the Goldstone–Canberra data arc on August 11 [note that in this figure, the cosine minima that occur in Eq. (4) have been suppressed, and only the envelope of the theoretical spectrum is shown]. The experimental and theoretical spectra are qualitatively similar, though the experimental spectrum is not as strongly suppressed at low frequencies as is the theoretical spectrum. Other error sources in addition to solar plasma may be increasing the magnitude of the experimental spectrum at the lowest frequencies. Both spectra have a "knee" at close to 0.01 Hz (note that $v_{sw}/S = 0.013$ Hz). The theoretical spectrum is about one order of magnitude larger than the experimental spectrum for higher frequencies; this is consistent with the factor of 3 difference between the predicted phase error and scatter of the SBI residuals at short averaging intervals. This discrepancy could reflect either daily variation in the solar wind turbulence or it may suggest that the model for plasma-induced doubly differenced phase scintillations needs to be renormalized. The acquisition of additional data, particularly dual-band data, is needed to help resolve this issue. Figure 8 also shows the predicted spectra of the errors due to system thermal noise and the ionosphere. The measured spectrum is in good agreement with the predicted system noise effect at the highest frequencies. The ionospheric error spectrum was computed assuming white frequency noise for lower frequencies and Kolmogorov turbulence for higher frequencies, with a magnitude consistent with the error budget. The ionosphere may be affecting the measured spectrum at the lowest frequencies.

The measured spectrum of SBI data residuals and the spectra of predicted error sources are shown in Fig. 9 for

its medium gain antenna, and the predicted solar plasma and ionospheric errors are less for February 20, since the angular separation between the two spacecraft was smaller during the February 20 SBI data arc. The measured spectrum is again in qualitative agreement with the prediction, which suggests that error models have been successfully applied for two different observation geometries.

The SBI measurement error as a function of averaging interval is displayed in Fig. 10. Curves are drawn for the predicted error for both the August 1990 and the February 1991 data sets. Points are plotted for the errors as measured for the August 11 and the February 20 data arcs. The measured values are about 25 percent less than predicted for 5-min averages, and about a factor of three less than predicted for shorter averaging intervals. Good characterization of measurement errors is more important at the longer averaging intervals, since orbit determination will be affected by the errors which remain after data averaging.

It should be noted that in acquiring the SBI data, the signals are not simultaneously recorded; the spacecraft signals from the two spacecraft are recorded in separate channels which are multiplexed with 1-sec dwells. Time multiplexing of the channels can conceivably introduce additional instrumental phase errors that do not cancel when the spacecraft signals are doubly differenced. For this reason, several phase calibration tones are injected near the beginning of the instrumental path into each channel. The phase calibration tone generator is locked to the station's hydrogen maser, providing frequency stability at the level of 10^{-15} sec/sec for 1000-sec intervals. Calculation of the power spectrum of doubly differenced phase calibration tone residuals for the August 1990 data set showed that the errors contributed by imperfect instrumental cancellation between channels was insignificant; the power spectrum of doubly differenced phase calibration tone residuals was several orders of magnitude below the measured spectrum illustrated in Fig. 8.

VI. Discussion

The SBI data acquired in 1990–1991 from the Magellan and Pioneer 12 orbiters at Venus have provided an initial assessment of SBI measurement errors. The scatter in the residuals is consistent with predictions for averaging intervals of 5 min, and less than predicted by about a factor of 3 for shorter averaging intervals. The error budget for these measurements, made at S-band, is entirely dominated by solar plasma fluctuations at the shorter averaging intervals. The plasma error model is based on line-of-sight observations. The eventual availability of dual-frequency same-beam radio metric data is expected to provide substantial improvement of this model for predicting SBI errors.

A single S-band SBI measurement (5-min average) determines spacecraft plane-of-sky separation with an accuracy of 40 to 100 m. Measurements made at X-band are expected to be more accurate by an order of magnitude. Measurement errors other than solar plasma are not distinguishable in the available S-band data set. Additional data acquisition is anticipated to further examine measurement system errors.

Demonstration of improved orbital accuracy is essential to validate the performance of the SBI measurement technique. Orbits generated using disjointed data arcs, and various combinations of Doppler, differenced Doppler, and SBI data, may be propagated to a common epoch and compared. The radio metric data in hand from Magellan and Pioneer 12 provide the opportunity to demonstrate the contribution of the SBI technique toward orbital accuracy improvement.

Acknowledgments

The authors thank the Magellan and Pioneer projects for their cooperation and support in obtaining the radio metric data analyzed here. The reference spacecraft trajectories used in this analysis were supplied by the Magellan and Pioneer navigation teams.

References

[1] J. R. Smith and R. Ramos, "Data Acquisition for Measuring the Wind on Venus from Pioneer Venus," *IEEE Transactions on Geoscience and Remote Sensing*, vol. GE-18, no. 1, pp. 126–130, January 1980.

[2] R. A. Preston, C. E. Hildebrand, G. H. Purcell, Jr., J. Ellis, C. T. Stelzried, S. G. Finley, R. Z. Sagdeev, V. M. Linkin, V. V. Kerzhanovich, V. I. Altunin, L. R. Kogan, V. I. Kostenko, L. I. Matveenko, S. V. Pogrebenko, I. A. Strukov, E. L. Akim, Yu. N. Alexandrov, N. A. Armand, R. N. Bakitko, A. S. Vyshlov, A. F. Bogomolov, Yu. N. Gorchankov, A. S. Selivanov, N. M. Ivanov, V. F. Tichonov, J. E. Blamont, L. Boloh, G. Laurans, A. Boischot, F. Biraud, A. Ortega-Molina, C. Rosolen, and G. Petit, "Determination of Venus Winds by Ground-Based Radio Tracking of the VEGA Balloons," *Science*, vol. 231, pp. 1414–1416, March 21, 1986.

[3] C. C. Counselman III, H. F. Hinteregger, and I. I. Shapiro, "Astronomical Applications of Differential Interferometry," *Science*, vol. 178, pp. 607–608, November 10, 1972.

[4] R. W. King, C. C. Counselman III, and I. I. Shapiro, "Lunar Dynamics and Selenodesy: Results from Analysis of VLBI and Laser Data," *J. Geophys. Res.*, vol. 81, no. 35, pp. 6251–6256, December 10, 1976.

[5] J. S. Border and R. D. Kahn, "Relative Tracking of Multiple Spacecraft by Interferometry," in *Advances in the Astronautical Sciences: Orbital Mechanics and Mission Design*, vol. 69, edited by J. Teles, San Diego, California: Univelt, 1989.

[6] J. S. Border and W. M. Folkner, "Differential Spacecraft Tracking by Interferometry," *Proceedings of the CNES International Symposium on Space Dynamics*, Toulouse, France, November 1989.

[7] W. M. Folkner and J. S. Border, "Orbiter–Orbiter and Orbiter–Lander Tracking Using Same-Beam Interferometry," *TDA Progress Report 42-109*, vol. January–March 1992, Jet Propulsion Laboratory, Pasadena, California, pp. 74–86, May 15, 1992.

[8] R. D. Kahn, W. M. Folkner, C. D. Edwards, and A. Vijayaraghavan, "Position Determination of a Lander and Rover at Mars With Earth-Based Differential Tracking," *TDA Progress Report 42-108*, vol. October–December 1991, Jet Propulsion Laboratory, Pasadena, California, pp. 279–293, February 15, 1992.

[9] D. B. Engelhardt, J. B. McNamee, S. K. Wong, F. G. Bonneau, E. J. Graat, R. J. Haw, G. R. Kronschnabl, and M. S. Ryne, "Determination and Prediction of Magellan's Orbit," paper AAS-91-180, AAS/AIAA Spaceflight Mechanics Meeting, Houston, Texas, February 11–13, 1991.

[10] W. G. Melbourne and D. W. Curkendall, "Radio Metric Direction Finding: A New Approach to Deep Space Navigation," paper presented at AAS/AIAA Astrodynamics Specialist Conference, Jackson Hole, Wyoming, September 7–9, 1977.

[11] S. W. Thurman, "Deep-Space Navigation with Differenced Data Types, Part II: Differenced Doppler Information Content," *TDA Progress Report 42-103*, vol. July–September 1990, Jet Propulsion Laboratory, Pasadena, California, pp. 61–69, November 15, 1990.

[12] K. M. Liewer, "DSN Very Long Baseline Interferometry System Mark IV-88," *TDA Progress Report 42-93*, vol. January–March 1988, Jet Propulsion Laboratory, Pasadena, California, pp. 239–246, May 15, 1988.

[13] J. S. Border and E. R. Kursinski, "Deep Space Tracking and Frequency Standards," *Proceedings of the 45th Annual Symposium on Frequency Control*, IEEE Catalog No. 91CH2965-2, Los Angeles, California, May 29–31, 1991.

[14] C. Dunn, S. Lichten, D. Jefferson and J. S. Border, "Sub-Nanosecond Clock Synchronization and Precision Deep Space Tracking," *Proceedings of the Twenty-Third Annual Precise Time and Time Interval (PTTI) Applications and Planning Meeting*, Pasadena, California, December 3–5, 1991.

[15] N. C. Ham, "VLBI System (BLK I) IF-Video Down Conversion Design," *TDA Progress Report 42-79*, vol. July–September 1984, Jet Propulsion Laboratory, Pasadena, California, pp. 172–188, November 15, 1984.

[16] A. P. Freedman, "Combining GPS and VLBI Earth-Rotation Data for Improved Universal Time," *TDA Progress Report 42-105*, vol. January–March 1991, Jet Propulsion Laboratory, Pasadena, California, pp. 1–12, May 15, 1991.

[17] U. J. Lindqwister, A. P. Freedman, and G. Blewitt, "A Demonstration of Centimeter-Level Monitoring of Polar Motion With the Global Positioning System," *TDA Progress Report 42-108*, vol. October–December 1991, Jet Propulsion Laboratory, Pasadena, California, pp. 1–9, February 15, 1992.

[18] M. H. Finger and W. M. Folkner, "A Determination of the Radio-Planetary Frame Tie From Comparison of Earth Orientation Parameters," *TDA Progress Report 42-109*, vol. January–March 1992, Jet Propulsion Laboratory, Pasadena, California, pp. 1–21, May 15, 1992.

[19] R. N. Treuhaft and G. E. Lanyi, "The Effect of the Dynamic Wet Troposphere on Radio Interferometric Measurements," *Radio Science*, vol. 22, no. 2, pp. 251–265, March–April 1987.

[20] R. Woo and J. W. Armstrong, "Spacecraft Radio Scattering Observations of the Power Spectrum of Electron Density Fluctuations in the Solar Wind," *J. Geophys. Res.*, vol. 84, no. A12, pp. 7288–7296, December 1, 1979.

[21] R. D. Kahn and J. S. Border, "Precise Interferometric Tracking of Spacecraft at Low Sun–Earth–Probe Angles," paper AIAA-88-0572, AIAA 26th Aerospace Sciences Meeting, Reno, Nevada, January 11–14, 1988.

[22] R. Woo, F.-C. Yang, K. W. Yip, and W. B. Kendall, "Measurements of Large-Scale Density Fluctuations in the Solar Wind Using Dual-Frequency Phase Scintillations," *Astrophysical J.*, vol. 210, pp. 568–574, December 1, 1976.

Table 1. Pioneer 12 and Magellan transmitter frequencies.

Transmitter frequency, MHz	S-band	X-band
Radio frequency	2293.81	8410.63
Frequency offset	4.16	0.11

Table 2. SBI measurement error model assumptions.

Source	Magnitude
Station clock offset	0.1 μsec
Zenith troposphere error	4 cm
Zenith ionosphere error	5 TEC units
Baseline component error[a]	21.2 cm

[a] Includes station location, Earth orientation, and radio-planetary frame tie.

Table 3. SBI observation geometry.

Component	August 1990	February 1991
Venus		
Right ascension, deg	120.3	355.7
Declination, deg	20.8	−3.2
Sun–Earth–Venus angle, deg	21.3	25.8
Distance from Earth, AU	1.563	1.472
Elevation angle, deg		
Madrid	15.	—
Goldstone	45.	20.
Canberra	15.	35.
Differential elevation angle, mrad		
Madrid	0.16	—
Goldstone	0.30	0.07
Canberra	0.16	0.07
Angular separation, mrad		
Goldstone–Madrid	0.30	—
Goldstone–Canberra	0.24	0.09
Change in S-band Doppler shift over data arc, kHz		
Magellan	47.	54.
Pioneer 12	2.4	67.

Table 4. PVO and MGN link analysis, for PVO S-band and X-band carriers, MGN S-band carrier from medium-gain antenna (MGA) and high-gain antenna (HGA), and MGN -16th harmonic of high-rate telemetry subcarrier at X-band.

Link component	PVO S-band	PVO X-band	MGN S-band MGA	MGN S-band HGA	MGN X-band
Power transmitted, dBm	40.0	27.8	35.5	35.6	42.4
Spacecraft antenna gain, dB	25.2	35.0	18.7	35.9	47.9
Space loss, 1.5 AU, dB	−267.1	−278.3	−267.1	−267.1	−278.3
P_{Tone}/P_{Total}, dB	−8.4	0.0	−3.5	−7.4	−38.1
Polarization loss, dB	0.0	0.0	−0.5	−3.0	0.0
Receiving antenna gain, dB	56.0	68.0	56.0	56.0	68.0
P_{Tone}, dBm	−154.3	−147.5	−160.9	−150.0	−158.1
N_0[a], dBm/Hz	−182.1	−184.6	−182.1	−182.1	−184.6
P_{Tone}/N_0, dB·Hz	27.8	37.1	21.2	32.1	26.5
P_{Tone}/N_0, W/W	603.	5130.	132.	1620.	447.
$SNR_{V,1sec}$	27.7	80.8	13.0	45.4	23.9

[a] System temperature 45 K at S-band and 25 K at X-band.

Table 5. SBI data acquired from Magellan and Pioneer 12.

Session	Goldstone–Madrid, hr	Goldstone–Canberra, hr	Radio frequency, GHz
August 1990	2	3	2.3
February 1991	0	8	2.3
April 1991	7	13.5	2.3

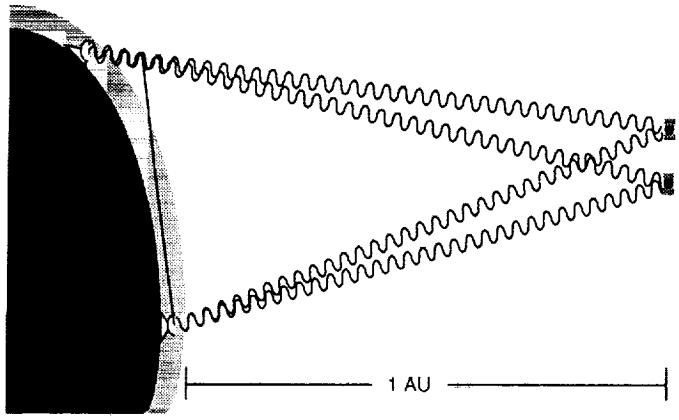

Fig. 1. Geometry of SBI measurements.

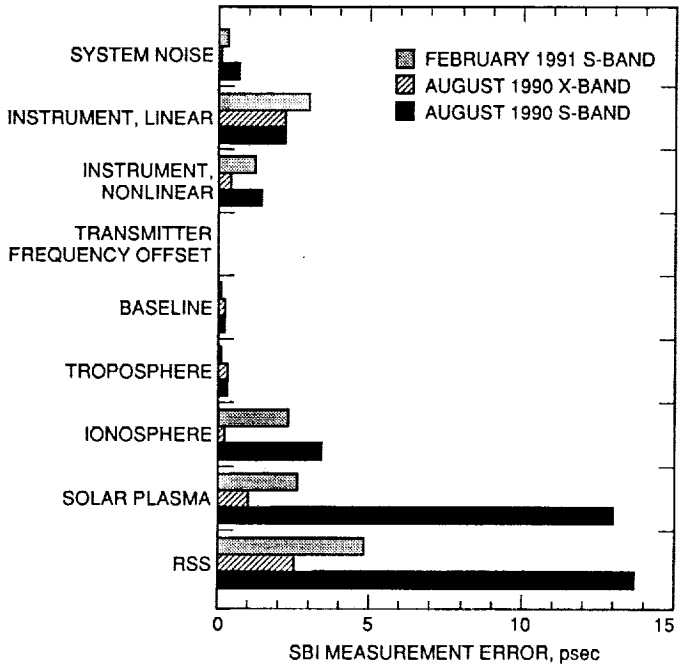

Fig. 2. Predicted SBI measurement errors for MGN–PVO for 5-min averages. Predicted X-band errors are shown for comparison only.

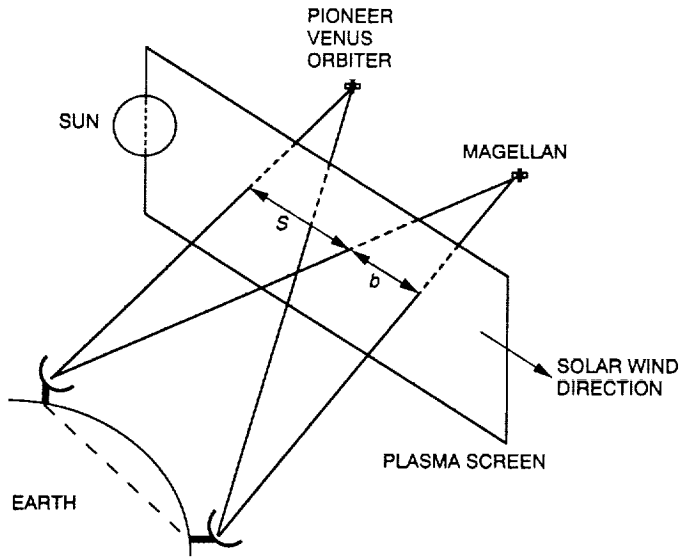

Fig. 3. Geometry of radio signals traversing the solar plasma.

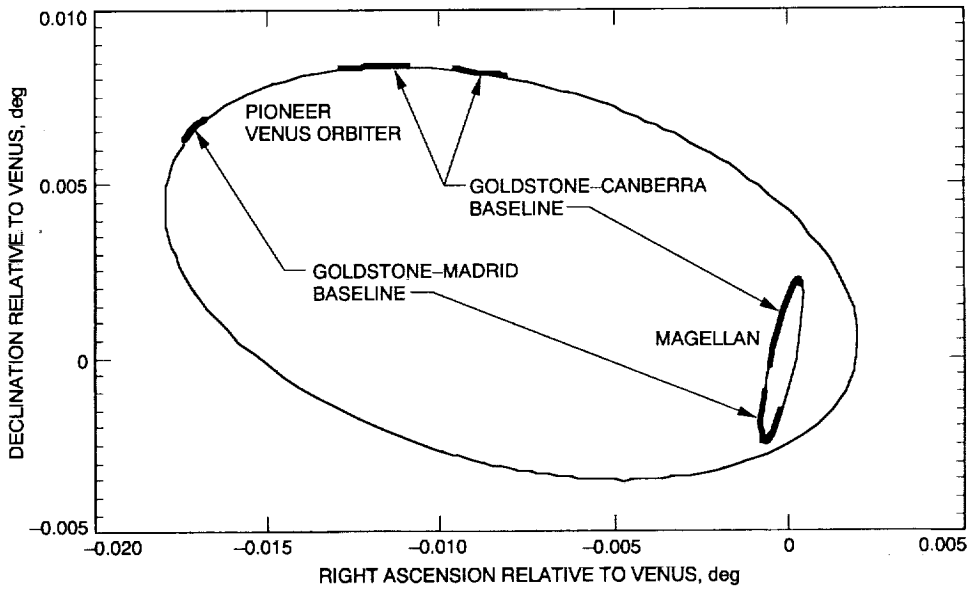

Fig. 4. Venus-centered orbit traces of MGN and PVO as seen from Earth, for geometry of August 1990.

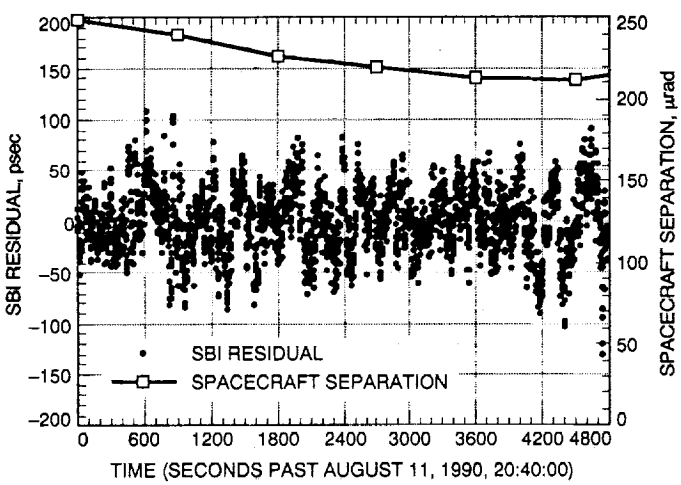

Fig. 5. Two-second MGN–PVO SBI residuals (S-band) for Goldstone–Canberra, August 11, 1990.

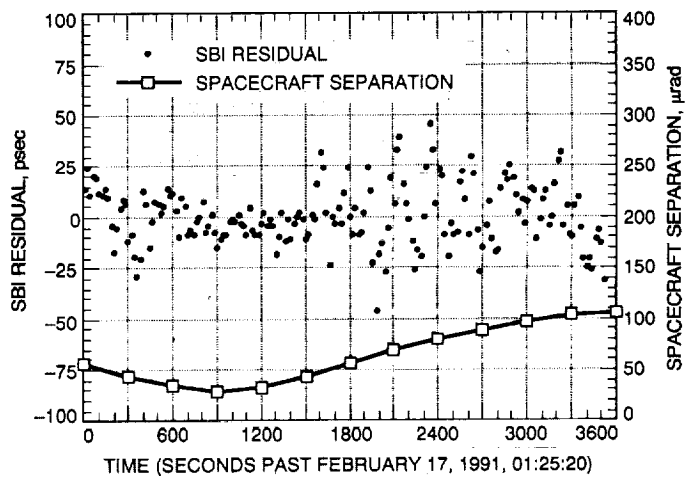

Fig. 6. Twenty-second MGN–PVO SBI residuals (S-band) for Goldstone–Canberra, February 17, 1991.

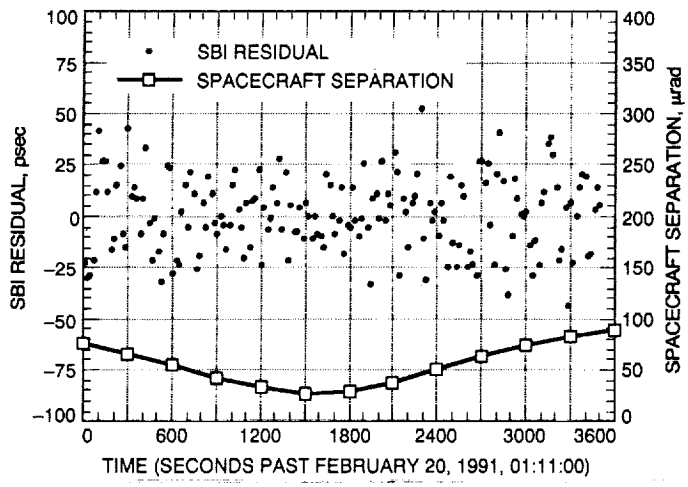

Fig. 7. Twenty-second MGN–PVO SBI residuals (S-band) for Goldstone–Canberra, February 20, 1991.

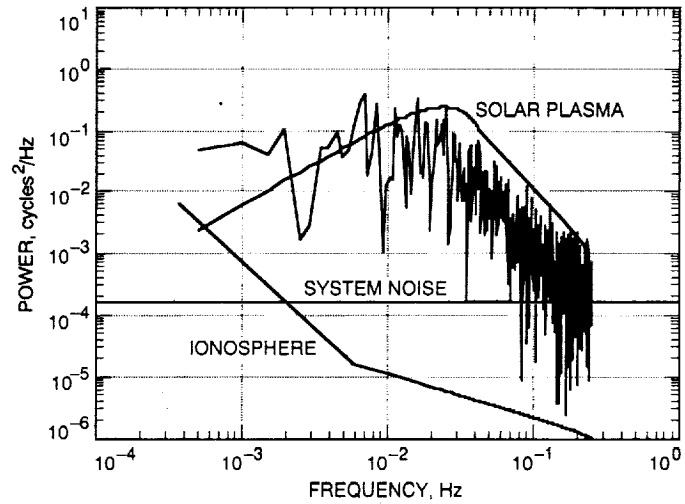

Fig. 9. Power spectrum of doubly differenced residual phase (S-band), observed and predicted, for Goldstone–Canberra, February 20, 1991.

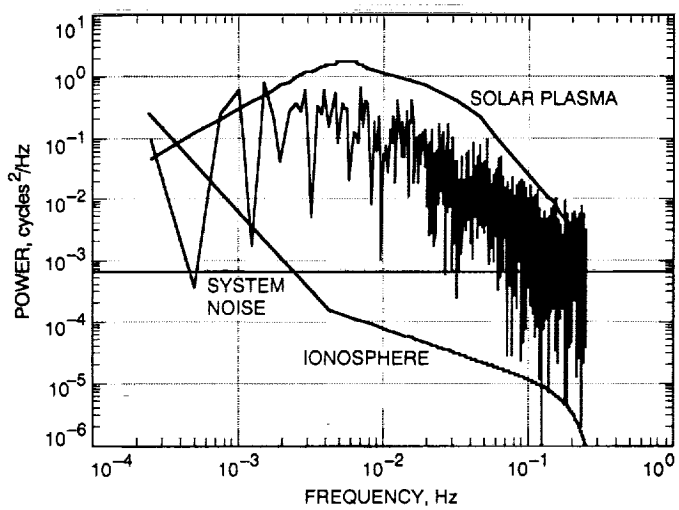

Fig. 8. Power spectrum of doubly differenced residual phase (S-band), observed and predicted, for Goldstone–Canberra, August 11, 1990.

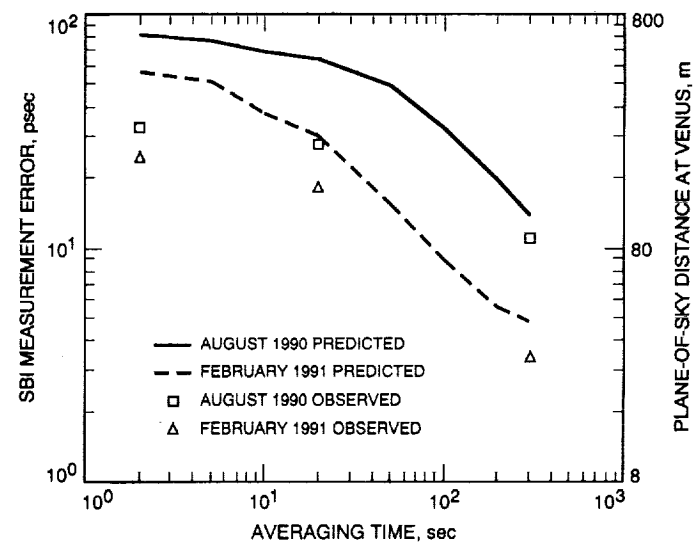

Fig. 10. Observed and predicted SBI measurement error (S-band) as a function of averaging interval.